Synthetic Metals 162 (2012) 1364–1368

Contents lists available at SciVerse ScienceDirect

Synthetic Metals

journal homepage: www.elsevier.com/locate/synmet

# Transparent conducting films based on graphene oxide/silver nanowire hybrids with high flexibility

Young Soo Yun, Do Hyeong Kim, Bona Kim, Hyun Ho Park, Hyoung-Joon Jin*

*Department of Polymer Science and Engineering, Inha University, Incheon 402-751, Republic of Korea*

ARTICLE INFO

*Article history:*
Received 24 April 2012
Received in revised form 24 May 2012
Accepted 28 May 2012
Available online 4 July 2012

*Keywords:*
Graphene oxide
Silver nanowire
Transparent conducting films

ABSTRACT

Transparent conducting films (TCFs) with high flexibility were successfully prepared by using graphene oxide (GO) and silver nanowire (Ag NW) hybrids. Forty-nanometerthick GO layers were coated on three different substrates, polyethylene terephthalate, glass and quartz, by capillary flow as a driving force during solvent evaporation of GO dispersions. Ag NW networks were formed on the GO layers by electrostatic force by dip coating. Melting and fusion of the Ag NWs after thermal annealing dramatically increased their contacts to the GO layers, resulting in mechanically stable and flexible TCFs with a transmittance of 86% and a sheet resistance of 150 Ω/□, which is comparable to indium tin oxide.



## 1. Introduction

Transparent conductive films (TC films) are essential to many areas of modern electronics and have been widely used in applications such as touch screens, organic light emitting diodes, flat panel displays, and solar cells [1]. Typically, indium tin oxide (ITO) has been used in TC films for its excellent transparency throughout the visible spectrum, its relatively low sheet resistance, and the compatibility of its work function with the injection and collection of charge carriers in organic semiconductors. However, it has three disadvantages: (1) ITO is inherently inefficient with plastic substrates because of its high temperature processing, (2) the high material cost, and (3) ITO cannot be used in flexible TC films because of its brittle nature [2–4]. Therefore, ITO substitutes need to be developed for the electronic industry. Several groups have investigated various materials as potential ITO replacements for TC films with similarly high performance [5–15]. Among several materials, silver nanowires (Ag NWs) with a high aspect ratio, which have the highest electrical conductivity ($6.3 \times 10^7$ S/m) among all the metals, are considered very promising candidates for use in flexible electronics [13,14].

Graphene, a new class of two-dimensional carbon nanostructure, has attracted considerable attention owing to its unique electrical properties, such as high carrier mobility [16], an ambipolar field effect [17] and a quantum hall effect [18]. Graphene oxide (GO), which contains numerous oxygen functional groups, is easily available through the controlled chemical oxidation of graphite. These oxygen functional groups render GO stable and induce homogeneous colloidal suspensions in aqueous and various polar organic solvents. In addition, the polar site of GO can induce a strong electrostatic interaction between it and the metal. Two papers have reported a strong interaction between graphene and silver [19,20]. However, few studies have investigated TC films using silver-supported graphene. A droplet of GO nanocolloids tends to leave the typical "coffee ring stain" type of drying pattern, just as in common water-soluble or dispersible materials [21,22]. Such ring deposits are common wherever drops containing dispersed solids evaporate on a surface, and they influence processes such as printing, washing and coating.

The goal of this study was to fabricate competitive TC films with high mechanical stability using Ag NWs and GO. For the fabrication of nanothick graphene layers, we introduced a new method that uses capillary flow as a driving force during solvent evaporation of GO dispersions. We used this new method in tandem with a simple and eco-friendly process to manufacture three substrates: polyethylene terephthalate (PET), glass and quartz. Ag NW networks were formed on the GO layers by repetitive dip coating because the GO layers have an electrostatic interaction with Ag NWs. Adhesion between the Ag NW networks and GO layers was greatly enhanced after thermal annealing at 150 °C. The resulting TC films exhibited good flexibility, high mechanical stability and superior TC film performance with a transmittance of 86% and a sheet resistance of 150 Ω/□, which is comparable to ITO.

* Corresponding author. Tel.: +82 32 860 7483; fax: +82 32 865 5178.
*E-mail address:* hjjin@inha.ac.kr (H.-J. Jin).

0379-6779/$ – see front matter © 2012 Elsevier B.V. All rights reserved.
http://dx.doi.org/10.1016/j.synthmet.2012.05.026

## 2. Experimental

### 2.1. Preparation of aqueous GO dispersions

GO was prepared from natural graphite (Sigma–Aldrich) using the Hummers method. Aqueous GO suspensions were frozen in liquid nitrogen and then freeze-dried with a lyophilizer (LP3, Jouan, France) at −50 °C and 0.045 mbar for 72 h to obtain low density, loosely packed GO powders [23]. Then, 2 mg of GO powders was exfoliated by ultrasonication in 1000 ml of deionized water.

### 2.2. Synthesis of Ag NWs

Ag NWs were synthesized by reducing $AgNO_3$ with ethylene glycol (EG) in the presence of polyvinylpyrrolidone (PVP). In a typical experimental procedure, 10 ml of $AgNO_3$ solution (0.1 M, in EG) was heated in a three-necked flask at 160 °C, and then 1 ml of NaCl solution (1.7 mM, in EG) was quickly added. After reacting for 15 min, the PVP solution (0.15 M, in EG) was injected drop-wise into the reaction system by syringe for 10 min. The reaction was kept at 160 °C for another 2 h, and magnetic stirring was maintained during the entire procedure. After the solution was cooled to room temperature, the final dispersion was diluted with acetone and centrifuged at 4000 rpm for 30 min. After centrifugation, the supernatant dissolved residual EG was removed by syringe. Then water was added into the centrifuge tube to disperse the products and to dissolve the residual PVP. After centrifugation, the supernatant was also removed by syringe, and the process was repeated twice more. These purified products were preserved in a vacuum oven.

### 2.3. Preparation of electrically conductive and transparent (TC) films

Glass, quartz and PET substrates were dipped in the aqueous GO dispersions (0.0002 wt%) and then allowed to stand for 24 h at 333 K in an oven. Following water evaporation, GO layers were deposited on the substrates. After being pulled up, the substrates were dried in a vacuum oven thoroughly. Then, a dip coating method was used to transfer the Ag NWs into the GO on the substrates by vertically dipping the GO-coated substrates into the Ag NW dispersion and pulling them up. After repeated dip coating of the GO-coated substrates, the GO layers containing Ag NW networks were dried in a vacuum oven. Finally, the GO/Ag NW hybrid TC films were annealed in a tube furnace at 150 °C for 30 min in an oxygen atmosphere to maximize adhesion between the Ag NWs and GO and to remove the remaining PVP layers on the surface of the Ag NWs.

### 2.4. Characterization

After the samples were pre-coated with a homogeneous Pt layer through ion sputtering (E-1030, Hitachi, Japan), the surface morphology of the hybrid films was observed by field-emission scanning electron microscopy (FESEM, S-4300SE, Hitachi, Japan) at an accelerating voltage of 15 kV. The topological characteristics of the GO layers were observed by atomic force microscopy (AFM, SPA400, Seiko Ins., Japan) operated in tapping mode. X-ray photoelectron spectroscopy (XPS, PHI 5700 ESCA) was performed using monochromated Al Kα radiation ($h\nu$ = 1486.6 eV). An Agilent 8453 UV-visible spectrophotometer (Agilent Technologies, Germany) was used to measure the transmittances of the TC films in a wavelength range from 380 to 750 nm. A four-probe method with an electrical conductivity meter (Loresta GP, Mitsubishi Chemical, Japan) was used to measure the electrical conductivity of the hybrid nano-films.

## 3. Results and discussion

To prepare a nanothick GO film, we used a new method in which a substrate was coated by capillary flow as a driving force. When the solvent evaporated, a capillary flow was generated in the substrate–liquid interface [21]. The capillary flow enabled formation of a nano-scale GO film in the substrate–liquid interface from GO nanocolloids. In addition, the film thickness could be controlled by varying the evaporation rate and concentration of the GO nanocolloids [21]. Fig. 1 shows the mechanism of nanothick GO film formation. When the solvent was evaporated in the interface between the GO nanocolloids and the substrate, which was dipped in a beaker vertically, a capillary flow was generated into the edge. As the water level decreased due to the evaporation of the solvent, GO was continuously deposited onto the substrate.

Fig. 2 shows the surface morphologies of the GO films deposited on a PET substrate from water dispersion. The GO films had a wide range of wrinkled surface and a thickness of around 40 nm (Fig. 2(a) and (b)). The specific morphological characteristics of the local area were investigated using AFM. The surface composed of several GO layers exhibited corrugation patterns that were similar to those observed during the evaporation of the polymer solutions. In surface morphologies of thin films prepared by evaporation of polymer solutions, the corrugation wavelength and corrugation amplitude are affected by mechanical instabilities [24] and hydrodynamic convection [25]. Benard–Marangoni instabilities, which result from a temperature gradient or a concentration gradient on the free surface, play an important role in the surface corrugation [24]. Therefore, control of temperature and concentration, as well as the evaporation rate, is important to control the surface morphology of thin films. We experimentally determined the optimized concentration of GO nanocolloids and temperature in water. The corrugation patterns of the GO film prepared at a GO nanocolloid concentration of 0.0002 wt% at 60 °C in water exhibited a topological difference of about 15 nm (Fig. 2(c) and (d)). In the GO film, the polydisperse size distribution and ruffled morphological property of GO also played an important role in creating the corrugation patterns.

Fig. 3(a) shows SEM images of Ag NWs synthesized by a polyol process. The average length and diameter of the Ag NWs were $6.1 \pm 2.9$ μm and $76.5 \pm 2.4$ nm, respectively. To prepare the GO/Ag NW hybrid films, the Ag NWs were transferred to the GO on the substrates by vertically dipping the GO-coated substrate into the Ag NW dispersion and slowly pulling it up. Ag NWs were deposited on the GO surface by electrostatic interaction. The few Ag NW networks on the GO surface, shown in Fig. 3(b), facilitated the good electroconductivity of the GO/Ag NW hybrid films for application to TC films. To increase adhesion between the GO and Ag NWs, and to raise the electroconductivities of the Ag NWs through decomposition of the PVP and improved contact between the Ag NWs and GO, the GO/Ag NW hybrid TC films were annealed in a tube furnace at 150 °C for 30 min in an oxygen atmosphere. Fig. 3(c) and (d) shows front and rear SEM images after thermal annealing. The images show the melting and fusion of the Ag NWs, which improved the contact between them and the Ag NWs adhered on the GO surface, but not to the front. In addition, the Ag NWs became connected via junctions, which dramatically decreased the junction resistance [14]. The effect of the thermal annealing is schematically shown in Fig. 4.

Fig. 5 shows the high-resolution C 1s XP spectra of (a) the GO/Ag NW hybrid films after thermal annealing, and (b) the Ag 3d XP spectra of the GO/Ag NW hybrid films before and after thermal annealing. The C 1s XP spectrum of the GO/Ag NW hybrid films after thermal annealing shows a considerable degree of oxidation with four components corresponding to carbon atoms with different functional groups: non-oxygenated ring C, C in C—O bonds, carbonyl

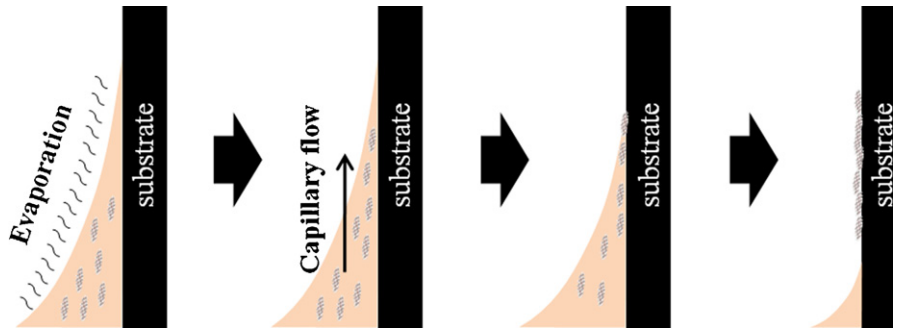


**Fig. 1.** Mechanism of nanothick GO film formation by capillary flow as a driving force.

C and carboxylated carbon (O—C═O) (Fig. 5(a)). The XP spectrum is similar to that of the original GO. This result suggests that GO was not reduced in the thermal annealing process in an oxygen atmosphere. The binding energy of Ag 3d for the GO/Ag NW hybrid film before thermal annealing was 368.1 eV (Fig. 5(b)), which is equal to that of pure Ag. This result confirms the absence of any interactions between the GO and Ag NWs before thermal annealing. However, the binding energy of Ag 3d for the GO/Ag NW hybrid film after thermal annealing was 367.5 eV, which was strongly shifted to a lower energy due to electron transfer from metallic Ag to the GO as a result of the work function difference between Ag (4.2 eV) and GO (4.48 eV) [20]. If the GO had been reduced, it would have reduced the transparency of the GO/Ag NW hybrid films. However, through thermal annealing, the Ag NWs became more strongly bound to the GO, and the junction resistance between the Ag NWs decreased without a reduction of GO. This result demonstrates that a few Ag NW networks binding the GO layer can produce mechanically stable and flexible TC films.

Fig. 6 shows the performances of the TC films with various substrates. The flexible TC film with the PET substrate exhibited a transmittance of 86% and a sheet resistance of 150 Ω/□. In addition, the TC films with different substrates exhibited a performance comparable to that of ITO. In particular, the sheet resistance of the TC film on a quartz substrate reached 40 Ω/□ when the transmittance was 86%. Furthermore, the transmittance of the TC film on a glass substrate reached 89% when the sheet resistance of the TC film was 200 Ω/□. The relative performance in terms of transparency and sheet resistance can be expressed numerically by the following equation.

$$\frac{\sigma_{DC}}{\sigma_{OP}} = \frac{Z_0}{2R_s(T^{-1/2}-1)} \quad (1)$$

where $Z_0 = 377\,\Omega$ is the impedance of the free space, $T$ is the transparency and $R_s$ is the sheet resistance. A high $\sigma_{DC}/\sigma_{OP}$ ratio indicates a high transmittance and a low sheet resistance. Table S1 shows the $\sigma_{DC}/\sigma_{OP}$ ratio of various GO- or Ag NW-based TC films prepared by different methods. Using Ag NWs only, the $\sigma_{DC}/\sigma_{OP}$ ratio of the TC films was relatively high compared to that of the GO-based TC film due to the superior electroconductivity of Ag NWs. In this study, the GO/Ag NW hybrid TC film had a $\sigma_{DC}/\sigma_{OP}$ ratio of 20.9–90, which is excellent considering its high mechanical stability and good flexibility.

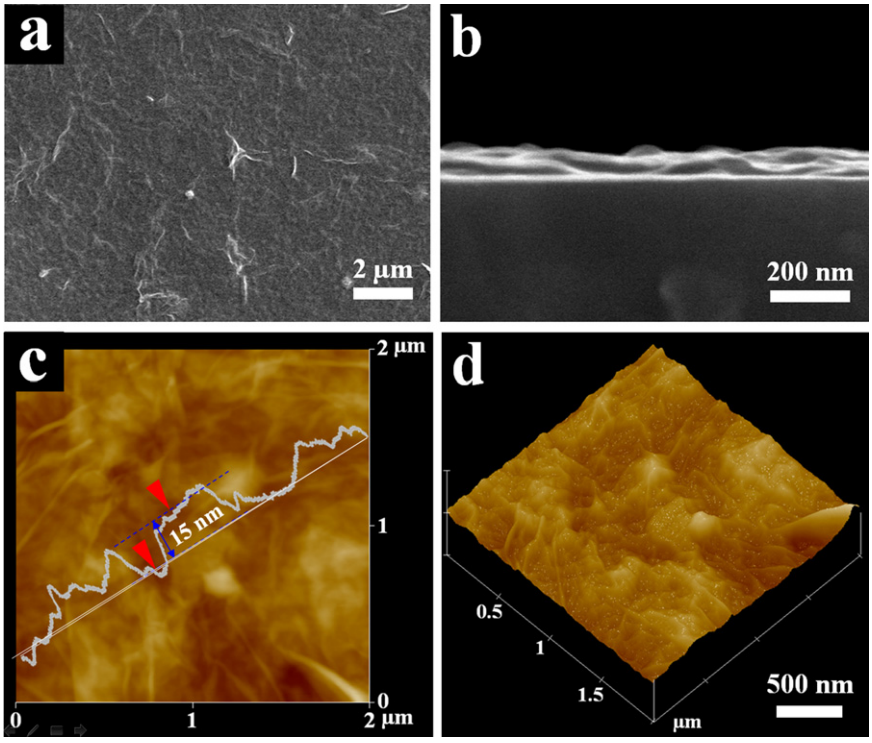


**Fig. 2.** (a) SEM image of a GO layer on a substrate, (b) SEM cross-sectional image of a GO layer, (c) AFM image of a GO layer and (d) 3D topological AFM image of a GO layer.

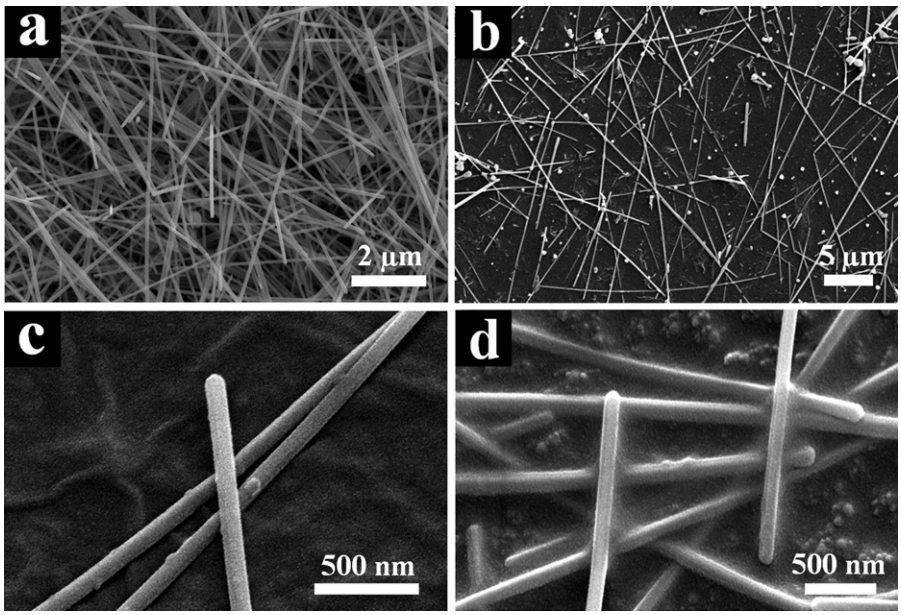


**Fig. 3.** SEM images of (a) Ag NWs synthesized by a polyol process, (b) Ag NW networks on a GO layer, (c) Ag NWs before thermal annealing and (d) Ag NWs after thermal annealing.

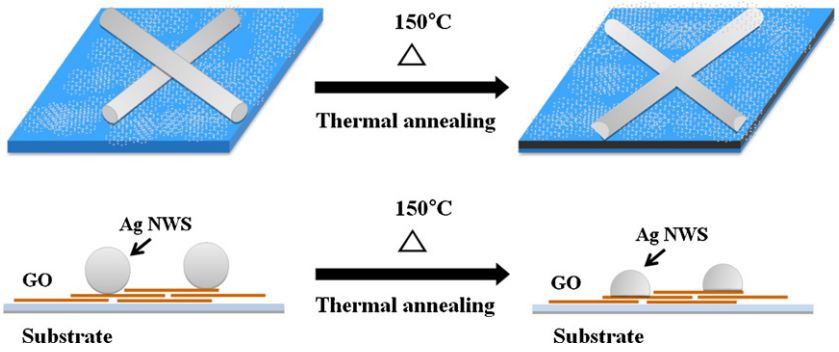


**Fig. 4.** Schematic image showing the effects of thermal annealing in the GO/Ag NW hybrid film.

Fig. 7 shows the flexible property of the GO/Ag NW hybrid TC film on a PET substrate. The sheet resistance of the film was maintained at a constant level during 500 cycles of bending test, which was attributed to the strong interaction between the GO and Ag NWs induced by thermal annealing. Moreover, an adherence test using sellotape confirmed the mechanical stability of the GO/Ag NW hybrid TC film (Fig. 8). The test was carried out by sticking sellotape to the film and then uncovering the sellotape from the film. The sample before thermal annealing made a stain on the sellotape but there was no stain on the sellotape after thermal annealing of the sample. This test confirmed the strong mechanical stability of the GO/Ag NW hybrid TC film.

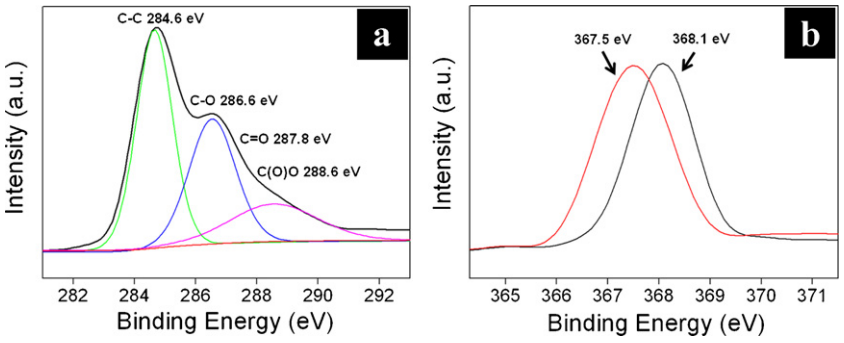


**Fig. 5.** (a) C 1s XP spectra of the GO/Ag NW hybrid film and (b) Ag 3d XP spectra of the GO/Ag NW hybrid film.

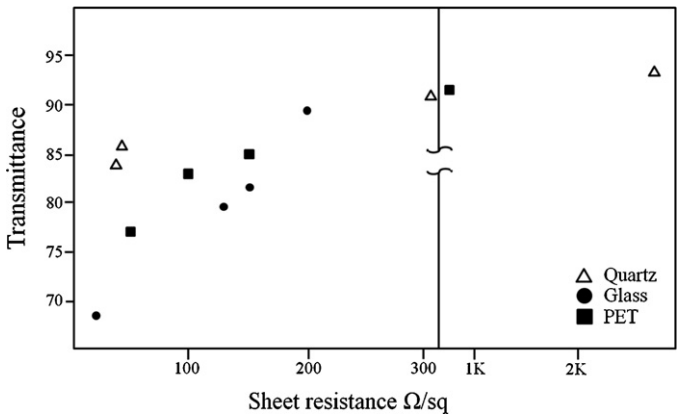


**Fig. 6.** Transmittance at 550 nm and sheet resistances for the GO/Ag NW hybrid films on three different substrates: PET, glass and quartz.

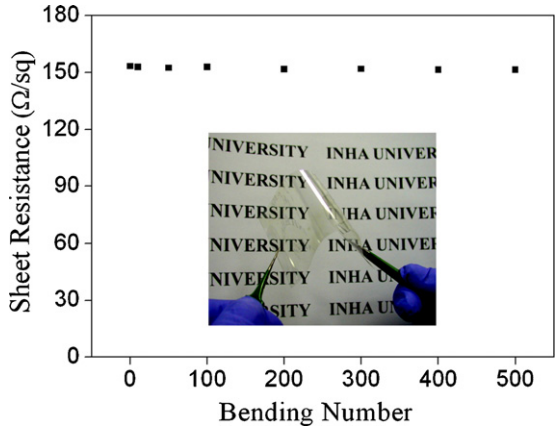


**Fig. 7.** Plot of the variation in the sheet resistance against the number of bending cycles for the GO/Ag NW hybrid film, with the insert showing the optical image of the flexible film.

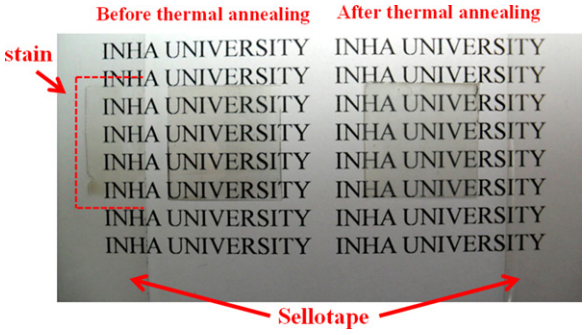


**Fig. 8.** Mechanical stability test using sellotape for the GO/Ag NW hybrid films before and after thermal annealing.

## 4. Summary

GO/Ag NW hybrid TC films were prepared using three different substrates: PET, glass and quartz. GO layers approximately 40 nm thick were coated on the substrates by capillary flow as a driving force during solvent evaporation. Ag NW networks were formed on the GO layers by electrostatic force using dip coating. The TC films with a PET substrate had good flexibility and high mechanical stability because of the strong interaction between the Ag NWs and GO after thermal annealing. The TC film with good flexibility and high mechanical stability exhibited a transmittance of 86% and a sheet resistance of 150 Ω/□, which is comparable to ITO.

## Acknowledgements

This research was supported by Basic Science Research Program through the National Research Foundation of Korea (NRF) funded by the Ministry of Education, Science and Technology (2011-0009614).

## Appendix A. Supplementary data

Supplementary data associated with this article can be found, in the online version, at http://dx.doi.org/10.1016/j.synthmet.2012.05.026.

## References

[1] Z. Wu, Z. Chen, X. Du, J.M. Logan, J. Sippel, M. Nikolou, K. Kamaras, J.R. Reynolds, D.B. Tanner, A.F. Hebard, Science 305 (2004) 1273–1276.
[2] R. Jackson, B. Domercq, R. Jain, B. Kippelen, S. Graham, Advanced Functional Materials 18 (2008) 2548–2554.
[3] J.-Y. Lee, S.T. Connor, Y. Cui, P. Peumans, Nano Letters 8 (2008) 689–692.
[4] E.M. Doherty, S. De, P.E. Lyons, A. Shmeliov, P.N. Nirmalraj, V. Scardaci, J. Joimel, W.J. Blau, J.J. Boland, J.N. Coleman, Carbon 47 (2009) 2466–2473.
[5] H. Tantang, A.K.K. Kyaw, Y. Zhao, M.B. Chan-Park, A.I.Y. Tok, Z. Hu, L.-J. Li, X.W. Sun, Q. Zhang, Chemistry: An Asian Journal 7 (2012) 541–545.
[6] A.K.K. Kyaw, H. Tantang, T. Wu, L. Ke, J. Wei, H.V. Demir, Q. Zhang, X.W. Sun, Journal of Physics D: Applied Physics 45 (2012) 165103.
[7] A.K.K. Kyaw, H. Tantang, T. Wu, L. Ke, C. Peh, Z.H. Huang, X.T. Zeng, H.V. Demir, Q. Zhang, X.W. Sun, Applied Physics Letters 99 (2011) 021107.
[8] H. Tantang, J. Xiao, J. Wei, M.B.E. Chan-Park, L.-J. Li, Q. Zhang, European Journal of Inorganic Chemistry 27 (2011) 4182–4186.
[9] K. Hoshino, N. Yazawa, Y. Tanaka, T. Chiba, T. Izumizawa, M. Kubo, ACS Applied Materials & Interfaces 2 (2010) 413–424.
[10] Z. Chen, W. Ren, L. Gao, B. Liu, S. Pei, H.-M. Cheng, Nature Materials 10 (2011) 424–428.
[11] Y. Zhu, Z. Sun, Z. Yan, Z. Jin, J.M. Tour, ACS Nano 5 (2011) 6472–6479.
[12] Y.Y. Huang, E.M. Terentjev, ACS Nano 5 (2011) 2082–2089.
[13] C.-H. Liu, X. Yu, Nanoscale Research Letters 6 (2011) 75–82.
[14] L. Hu, H.S. Kim, J.-Y. Lee, P. Peumans, Y. Cui, ACS Nano 4 (2010) 2955–2963.
[15] H. Wu, L. Hu, M.W. Rowell, D. Kong, J.J. Cha, J.R. Mcdonough, J. Zhu, Y. Yang, M.D. Mcgehee, Y. Cui, Nano Letters 10 (2010) 4242–4248.
[16] K. Bolotin, K. Sikes, Z. Jiang, M. Klima, G. Fudenberg, J. Hone, P. Kim, H. Stormer, Solid State Communications 146 (2008) 351–355.
[17] S. Latil, L. Henrard, Physical Review Letters 97 (2006) 36803.
[18] Y. Zhang, Y.-W. Tan, H.L. Stormer, P. Kim, Nature 438 (2005) 201–204.
[19] J. Lee, K.S. Novoselov, H.S. Shin, ACS Nano 5 (2011) 608–612.
[20] J. Li, C. Liu, Journal of Inorganic Chemistry 2010 (2010) 1244–1248.
[21] R.D. Deegan, O. Bakajin, T.F. Dupont, G. Huber, S.R. Nagel, T.A. Witten, Nature 389 (1997) 827–828.
[22] J. Luo, L.J. Cote, V.C. Tung, A.T.L. Tan, P.E. Goins, J. Wu, J. Huang, Journal of the American Chemical Society 132 (2010) 17667–17669.
[23] Y.S. Yun, Y.H. Bae, D.H. Kim, J.Y. Lee, I.-J. Chin, H.-J. Jin, Carbon 49 (2011) 3553–3559.
[24] N. Bassou, Y. Rharbi, Langmuir 25 (2008) 624–632.
[25] S. Sakurai, C. Furukawa, A. Okutsu, A. Miyoshi, S. Nomura, Polymer 43 (2002) 3359–3364.